IC/99/18

the
abdus salam
international
centre
for theoretical
physics

united nations
educational, scientific
and cultural
organization

international atomic
energy agency

SYNTHETIC TSUNAMI MAREOGRAMS FOR REALISTIC OCEANIC MODELS

Giuliano F. Panza

Fabio Romanelli

and

Tatiana B. Yanovskaya

IC/99/18

United Nations Educational Scientific and Cultural Organization
and
International Atomic Energy Agency
THE ABDUS SALAM INTERNATIONAL CENTRE FOR THEORETICAL PHYSICS

SYNTHETIC TSUNAMI MAREOGRAMS FOR REALISTIC OCEANIC MODELS

Giuliano F. Panza
Dipartimento di Scienze della Terra, Via E. Weiss 4, 34127 Trieste, Italy
and
The Abdus Salam International Centre for Theoretical Physics, SAND Group, Trieste, Italy,

Fabio Romanelli
Dipartimento di Scienze della Terra, Via E. Weiss 4, 34127 Trieste, Italy
and
CNR, Gruppo Nazionale per la Difesa dei Terremoti, Via Nizza 128, 00198 Rome, Italy

and

Tatiana B. Yanovskaya
Institute of Physics, St. Petersburg University,
Petrodvoretz, 198904 St. Petersburg, Russian Federation
and
The Abdus Salam International Centre for Theoretical Physics, SAND Group, Trieste, Italy.

Abstract

We study how the tsunami mode is generated by a scaled double-couple seismic source and how it propagates in realistic oceanic models. The method developed and used is the direct extension to tsunami waves, propagating in multilayered oceanic media, of the well–known Haskell method. The most intensive tsunamis may be expected from sources located in the deep-water parts of the ocean, within the crust. The extension to laterally heterogeneous structures, shows that if the thickness of the ocean liquid layer diminishes, the maximum amplitude of the tsunami wavetrain increases.

MIRAMARE – TRIESTE

March 1999

1. INTRODUCTION

If a seismic wave is propagating in solid media the main restoring force involved is the interaction between adjacent particles, i.e. the elastic force. When fluid media are considered this is no longer true and the restoring force is primarily due to gravity.

Among the gravity waves that can propagate near the oceanic surface the most important ones, due to their amplitudes, are the tsunamis. Such waves can be distinguished from other gravity waves for their genesis. Actually, tsunamis are more commonly generated by submarine earthquakes and then they can be considered as seismic sea waves (Ward, 1989). Due to their generation mechanism, periods and wavelengths associated with tsunamis are longer than those associated with ordinary sea waves, and for large submarine earthquakes their amplitudes can be very impressive especially when tsunamis approach the shorelines.

In this work we study how the tsunami mode is generated by a scaled double-couple seismic source and how it propagates in realistic models of oceanic media. Several authors attacked the problem of how the tsunami mode is excited by a seismic source for a fully coupled ocean and solid earth model. Pod'yapolsky (1968, 1970) is the first to consider tsunami mode as one of the normal modes of the earth. Ward (1980, 1981, 1982a, b) applies originally the free oscillations formalism for a finite body to a spherically symmetric oceanic model and he shows how the energy of a tsunami mode is partitioned among gravitational and elastic components for fluid and solid media. Comer (1984) considers the same problem but using a flat, laterally homogeneous, model of the earth. He studies the excitation of the tsunami mode as a propagating mode and then the theoretical development of the solution is different from Ward's (1980). Comer's (1984) method is based on a formalism similar to those used for the study of Rayleigh waves, but suffers from some limitations, e.g. the computed examples are for a half-space underlying a single incompressible liquid layer and the excitation problem is studied using a variational approach for a uniform ocean depth.

The method developed and used in this work is the direct extension to tsunami waves, propagating in multilayered oceanic media, of the well-known Haskell method (Haskell, 1953), which has been successfully employed for the study of Rayleigh and Love waves in multilayered structures and for the construction of broad-band synthetic seismograms (e.g. Panza, 1985; Panza and Suhadolc, 1987; Florsch et al., 1991). We solve the equations of elastic motion when a constant gravitational field acts in the downward direction in the multilayered fluid which is in welded contact with a multilayered solid half-space where we assume that only elastic forces act. In such a way we can use the efficient algorithms valid for flat, multilayered oceanic structures, for the production of synthetic mareograms due to the excitation, by seismic sources, of the tsunami mode propagating in oceanic structures. This method is then extended to laterally heterogeneous structures in order to study the effect of the variation of the ocean bottom.

Such realistic synthetic tsunami mareograms not only are important for a subsequent inversion process for some important physical parameters (see e.g. Ritsema et al., 1995), but they play a relevant role for a quick system of tsunami warning since a database of synthetic parameters (e.g. maximum height at different locations) can be constructed before the event occurs.

2. PHASE VELOCITIES AND EIGENFUNCTIONS OF TSUNAMI WAVES IN MULTILAYERED OCEANIC STRUCTURES

The mathematical formulation we adopt for the problem is similar to the one used by Comer (1984), with the exception that we take into account the elastic forces in the liquid medium in order to obtain the same form of solution for the displacement in the solid and liquid layers.

In order to take into account the effects due to the gravity and elastic forces we follow Pod'yapolsky (1968, 1970): the gravitational force is assumed to be uniform and acting in the vertical direction, i.e. $g\rho\mathbf{e}_z$, leading to a static displacement field, that may be regarded as an equilibrium state. The variation of this force due to

the dynamic displacement field, $\mathbf{u}(x,t)$, is caused only by the variation of the density, i.e. by $\frac{\Delta\rho}{\rho} = -\nabla\cdot\mathbf{u}$. Then the equations of motion can be written as:

$$\alpha^2\nabla(\nabla\cdot\mathbf{u}) - g\mathbf{e}_z\nabla\cdot\mathbf{u} = \frac{\partial^2\mathbf{u}}{\partial t^2} \qquad (1)$$

in the liquid layers, and

$$\alpha^2\nabla(\nabla\cdot\mathbf{u}) - g\mathbf{e}_z\nabla\cdot\mathbf{u} - \beta^2\nabla\times(\nabla\times\mathbf{u}) = \frac{\partial^2\mathbf{u}}{\partial t^2} \qquad (2)$$

in the solid layers, where α is the velocity of P-waves, β is the velocity of S-waves and $\mathbf{u} = (u, 0, w)$ is the displacement vector. Equations (1) and (2) can be derived from equation (8.59) of Aki & Richards (1980). In fact, in the equilibrium state, gravitational acceleration, g_0, and density, ρ_0, are constant, the gravity potential, U, is equal to $-g_0\rho_0 z$ and consequently the perturbation of U is $-g_0\rho_0 w$.

At the free-surface of the fluid the pressure p, that in the liquid is due both to the elastic force and to the hydrostatic pressure, has to vanish, i.e.:

$$p\left[z_{-\ell} + w(z_{-\ell})\right] = p(z_{-\ell}) + \left.\frac{dp}{dz}\right|_{z_{-\ell}} w_{-\ell} = -\rho_{-\ell}\alpha_{-\ell}^2\nabla\cdot\mathbf{u}_{-\ell} + \rho_{-\ell}g w_{-\ell}\big|_{z_{-\ell}} = 0 \quad (3)$$

where the second order terms are neglected.

At the interfaces between the liquid layers the pressure and the vertical component of motion have to be continuous. If the j-th and (j+1)-th liquid layers are considered, the continuity conditions should be satisfied at the perturbed interface, i.e. at $z=z_{-j}+w(z_{-j})$, but for the vertical component of displacement it is equivalent to consider the unperturbed interface, i.e. $z=z_{-j}$. The conditions of continuity between the j-th and (j+1)-th liquid layers give:

$$w_{-j}(z_{-j}) = w_{-j-1}(z_{-j}) \qquad (4)$$

$$-\rho_{-j}\alpha_{-j}^2\nabla\cdot\mathbf{u}_{-j} + \rho_{-j}gw_{-j}\Big|_{z_{-j}} = -\rho_{-j-1}\alpha_{-j-1}^2\nabla\cdot\mathbf{u}_{-j-1} + \rho_{-j-1}gw_{-j-1}\Big|_{z_{-j}}$$

At the liquid-solid boundary (0-th interface according to Figure 1), we have:

$$w_{-1}(z_0) = w_1(z_0) \tag{5a}$$

$$\rho_{-1}\alpha_{-1}^2\nabla\cdot\mathbf{u}_{-1}(z_0) = \sigma_1(z_0) \tag{5b}$$

$$0 = \tau_1(z_0) \tag{5c}$$

In condition (5b) the terms corresponding to the hydrostatic pressure are neglected since the vertical displacement in the solid is much smaller than that in the liquid and the gravity term in equation (2) will be later neglected; thus, σ_1 is the normal stress due only to the elastic forces.

At the interface between the m-th and the (m+1)-th solid layers all of the components of displacement and of stress are continuous, i.e.

$$\begin{aligned} w_m(z_m) &= w_{m+1}(z_m) \\ u_m(z_m) &= u_{m+1}(z_m) \\ \sigma_m(z_m) &= \sigma_{m+1}(z_m) \\ \tau_m(z_m) &= \tau_{m+1}(z_m) \end{aligned} \tag{6}$$

for $1 \le m \le N\text{-}1$.

The solution of the equation of motion in the j-th liquid layer, due to both elastic and gravitational forces, in terms of a harmonic wave propagating along the x axis, with angular frequency ω and phase velocity c, is:

$$u_{-j}(x,z,t) = -\frac{i\alpha_{-j}^2}{\omega c}\left[A_{-j}\exp\left(-\frac{\eta_{2(-j)}z}{\alpha_{-j}}\right) - B_{-j}\exp\left(-\frac{\eta_{1(-j)}z}{\alpha_{-j}}\right)\right]\exp[i(\omega t - kx)]$$

(7)

$$w_{-j}(x,z,t) = \frac{\alpha_{-j}}{\omega^2}\left[\eta_{1(-j)}A_{-j}\exp\left(-\frac{\eta_{2(-j)}z}{\alpha_{-j}}\right) - \eta_{2(-j)}B_{-j}\exp\left(-\frac{\eta_{1(-j)}z}{\alpha_{-j}}\right)\right]\exp[i(\omega t - kx)]$$

where k is the horizontal wavenumber, i is the imaginary unit and

$$\eta_{1(-j)} = -\omega\psi_{-j} - \frac{g}{2\alpha_{-j}}$$

$$\eta_{2(-j)} = \omega\psi_{-j} - \frac{g}{2\alpha_{-j}} \qquad (8)$$

$$\psi_{-j}^2 = \frac{\alpha_{-j}^2}{c^2} - 1 + \frac{g^2}{4\alpha_{-j}^2\omega^2}$$

The solution of the equation of motion in the m-th solid layer is:

$$u_m(x,z,t) = \left\{\frac{i\alpha_m^2}{\omega c}\left[C_m\exp\left(-\frac{\eta_{2m}z}{\alpha_m}\right) + D_m\exp\left(-\frac{\eta_{1m}z}{\alpha_m}\right)\right] + \right.$$
$$\left. -\frac{ir_{\beta m}\beta_m}{\omega}\left[E_m\exp\left(-\frac{\omega r_{\beta m}z}{\beta_m}\right) + F_m\exp\left(\frac{\omega r_{\beta m}z}{\beta_m}\right)\right]\right\}\exp[i(\omega t - kx)]$$

(9a)

$$w_m(x,z,t) = \left\{\frac{\alpha_m}{\omega^2}\left[-\left(\eta_{1m} + \frac{g\beta_m^2}{\alpha_m\left(\alpha_m^2 - \beta_m^2\right)}\right)C_m\exp\left(-\frac{\eta_{2m}z}{\alpha_m}\right) + \right.\right.$$
$$\left.\left. -\left(\eta_{2m} + \frac{g\beta_m^2}{\alpha_m\left(\alpha_m^2 - \beta_m^2\right)}\right)D_m\exp\left(-\frac{\eta_{1m}z}{\alpha_m}\right)\right] + \right.$$

where

$$r_{\beta m} = \begin{cases} i\left[1 - (\beta_m / c)^2\right]^{1/2} & \text{if } c > \beta_m \\ \left[(\beta_m / c)^2 - 1\right]^{1/2} & \text{if } c < \beta_m \end{cases} \qquad (10a)$$

Gravity has no effect on the shear waves (9a), and, as it easy to estimate that the effect of gravity on the total displacement is minor. Therefore in the following we neglect the gravity force in the equations of motion for the solid medium. The formulas (9a) then reduce to:

$$u_m(x,z,t) = \left\{ \frac{i\alpha_m^2}{\omega c}\left[C_m \exp\left(-\frac{\omega r_{\alpha m} z}{\alpha_m} \right) + D_m \exp\left(\frac{\omega r_{\alpha m} z}{\alpha_m} \right) \right] + \right.$$
$$\left. -\frac{i r_{\beta m}\beta_m}{\omega}\left[E_m \exp\left(-\frac{\omega r_{\beta m} z}{\beta_m} \right) + F_m \exp\left(\frac{\omega r_{\beta m} z}{\beta_m} \right) \right] \right\} \exp[i(\omega t - kx)] \qquad (9b)$$

$$w_m(x,z,t) = \left\{ \frac{r_{\alpha m}\alpha_m}{\omega}\left[C_m \exp\left(-\frac{\omega r_{\alpha m} z}{\alpha_m} \right) - D_m \exp\left(\frac{\omega r_{\alpha m} z}{\alpha_m} \right) \right] + \right.$$

where

$$r_{\alpha m} = \begin{cases} i\left[1 - (\alpha_m / c)^2\right]^{1/2} & \text{if } c > \alpha_m \\ \left[(\alpha_m / c)^2 - 1\right]^{1/2} & \text{if } c < \alpha_m \end{cases} \qquad (10b)$$

Introducing the boundary conditions (see Appendix A) the dispersion equation can be constructed and the eigenvalues determined following standard methods (see Appendix B).

Once the phase velocity is determined, the coefficients in the expressions (7) and (9) for the eigenfunctions may be determined by a recursive procedure. The coefficients for the fluid and the solid layers are calculated separately, each with its own arbitrary normalization. Then from any boundary condition at the liquid-solid boundary (for example corresponding to the continuity of the vertical displacement) they are reduced to the same normalization.

For the solid layers the equation (see Appendix B)

$$\mathbf{C}\mathbf{L}_1^{-1}\mathbf{D}_2\ldots\mathbf{D}_{N-1}\mathbf{L}_n\begin{pmatrix}C_N\\E_N\end{pmatrix}=0 \qquad (11)$$

is used for the calculation of the coefficients of the eigenfunctions in the half-space C_n, E_n. One of them may be assumed to be equal to 1 and the coefficients for the upper layers are determined using Haskell (1953) layer matrices up to the first solid layer.

For the fluid layers we start from the coefficients of the uppermost layer, which are determined from equation (3) corresponding to the condition of free surface :

$$\mathbf{S}_{-\ell}\begin{pmatrix}A_{-\ell}\\B_{-\ell}\end{pmatrix}=0 \qquad (12)$$

where the **S** matrix is defined in Appendix A. The coefficients for the lower liquid layers are determined recursively from the equation

$$\begin{pmatrix}A_{-j}\\B_{-j}\end{pmatrix}=\mathbf{L}_{-j}^{-1}\,\mathbf{L}_{-j-1}\mathbf{K}_{-j-1}\begin{pmatrix}A_{-j-1}\\B_{-j-1}\end{pmatrix} \qquad (13)$$

where the matrices **L** and **K** are defined in Appendix A. When the coefficients for the last (j=1) liquid layer are determined, the coefficients in the solid and in the fluid layers are matched by equating the vertical displacements at the liquid-solid boundary and from this condition the normalization coefficient, for all the liquid layers, can be determined.

3. TSUNAMI WAVES EXCITED BY SEISMIC SOURCES

Once the eigenvalues and the eigenfunctions are determined, it is possible to calculate the synthetic mareogram in a laterally homogeneous oceanic model,

due to the excitation of the tsunami mode by a double-couple seismic source, using the asymptotic expression for a harmonic wave (A.A.V.V., 1989):

$$\mathbf{U}(X,\varphi,z,\omega,t) = \frac{\exp(-i\pi/4)}{\sqrt{8\pi}} \frac{\exp[i\omega(t-\tau)]}{\sqrt{kJ}} \frac{\chi(h_s,\varphi)R(\omega)}{\sqrt{cv_gI_1}} \frac{\mathbf{u}(z,\omega)}{\sqrt{cv_gI_1}} \qquad (14)$$

where h_s is the focal depth (from the free surface), X is the epicentral distance, $\tau=X/c$ is the travel time, J=X is the geometrical spreading, φ is the strike-receiver angle, $\mathbf{u} = u\mathbf{e}_x + w\mathbf{e}_z$, $R(\omega) = |R(\omega)| \exp[i \arg(R(\omega))]$ is the Fourier transform of the source time function and $\chi(h_s,\varphi)$ represents the part of the excitation that is function of the strike-receiver angle and of the source depth, h_s. The source geometry, the complete expression of $\chi(h_s,\varphi)$ for a double couple point-source, and the limits of validity of (18) are given by Panza et al. (1973). The quantity I_1 is the energy integral (see equation (7.74) in Aki and Richards,1980).

For weakly laterally heterogeneous media the asymptotic expression for the harmonic wave is of the same form of (14) (A.A.V.V., 1989), the difference is that the third and the fourth factors in the right term of (18) should be calculated locally at the source and at the receiver respectively, and in the second factor τ and J have to be calculated for the laterally varying medium:

$$\mathbf{U}(X,\varphi,z,\omega,t) = \frac{\exp(-i\pi/4)}{\sqrt{8\pi}} \frac{\exp[i\omega(t-\tau)]}{\sqrt{kJ}} \left.\frac{\chi(h_s,\varphi)R(\omega)}{\sqrt{cv_gI_1}}\right|_s \left.\frac{\mathbf{u}(z,\omega)}{\sqrt{cv_gI_1}}\right|_r \qquad (15)$$

where the subscripts s and r mean that the quantities have to be calculated respectively at the source and at the receiver.

We assume that the structure is varying only along the direction of propagation, i.e. along the x-axis. This restriction is not important when the phase velocity is changing approximately linearly along the path. Actually, as is shown in Appendix C, the difference between the calculated geometrical spreading (and the calculated travel time) for our model and a model in which the angle between the direction of propagation and the direction of variation of the structure is not zero, is negligible for a wide range of angles. Therefore, in a 2-D medium the phase velocity, that enters in the calculation of τ and J, can be

considered a function of x only. Since c(x) cannot be computed exactly, we assume that c varies linearly between the values corresponding to the structural models limited by the vertical planes, parallel to the y-z plane, passing for $x=x_0(=0),x_1,...,x_n(=X)$ (see Figure 2.a). At each point x_i (i=1,...,n) the phase velocity of the tsunami mode $c_0, c_1,..., c_n$ can be evaluated using the formalism of Section 2. The formulas for τ and J are given in Appendix C.

4. EXAMPLES OF CALCULATION IN THE FREQUENCY DOMAIN

In Figure 3a are shown the amplitude spectra, for the radial and the vertical component of motion, calculated at a distance of 500 km from a double–couple source with a seismic-moment of 10^{13} Nm and a focal depth of 14 km from the free-surface (i.e. 10 km deep in the solid media). The strike-receiver angle corresponds to a maximum of the radiation pattern and this choice is used for all the computations. The structural model that is adopted in the computations correspond to the one used by Comer (1984): a 4 km liquid layer (α=1.5 km/s, ρ=1.0 g/cm^3) over a solid half-space with α=7.15 km/s, β=4.1 km/s, ρ=3.1 g/cm^3. A general characteristic is that the dip-slip mechanism (suffix ds in Figure 3a) is more effective in the generation of tsunami motion than strike-slip, while the radial component of motion is greater than the vertical one by about a factor of 3. In Figure 3b are shown the amplitude spectra for different thicknesses of the liquid layer: 4 km, 6 km and 8 km. The parameters of the solid half-space are the same as in Figure 3a, the focal mechanism considered is dip-slip, and the source is located 10 km deep in the solid layers. The most important effect is due to the dependence of the phase and the group velocities on the thickness of the water layer that is shown in Figure 4 (that can be compared with Figure 1 of Ward, 1980).

To study the effect of the layering of the solid structure, the source radiation spectra are calculated for three solid models: model 1 corresponds to the homogeneous half-space used by Comer (1984); model 2 is the same of model 1 with a sedimentary layer (α=3.5 km/s, β=1.0 km/s, ρ=1.5 g/cm^3) 1 km thick on top of the half-space; model 3 has a crustal layer (α=5.2 km/s, β=3.0 km/s, ρ=2.6

g/cm^3) 12 km thick, over the half-space (α=8.1 km/s, β=4.7 km/s, ρ=3.2 g/cm^3). The thickness of the ocean is fixed at 4 km, while the seismic source corresponds to a dip-slip focal mechanism. In Figure 5 are shown the amplitude spectra for the vertical component of motion, calculated using model 1 and model 3. The source-receiver distance is 500 km while two focal depths, 9 and 14 km are shown. While the influence of the source-receiver distance on the amplitude spectra is a scale factor, the combination of the source depth effect with the solid layering is more interesting. Figure 5 shows that the earthquakes within the crust can excite more intensively the tsunami mode than the deeper earthquakes and that the lower is the S-wave velocity at the depth of the source the larger is the excitation of the tsunami mode. Calculations carried out for various combinations of α and β, show that the parameter controlling the amplitude of the tsunami waves is the S-wave velocity rather than the P-wave velocity. For sources located below the sediment layer the differences in the amplitude spectra for the models 1 and 2 are negligible and in Figure 5 the curves calculated for Model 2 would exactly overlap those relative to Model 1. This can be explained comparing (see Figure 6a,b) the eigenfunctions for the three models as functions of depth. The frequency chosen (0.007 Hz, i.e. T=143 s) corresponds approximately to the maxima of the amplitude spectra shown in Figure 5. The curves shown in Figure 6 are in good agreement with those shown by Ward (1980; Figures 3 and 4) for a period of 150 s.

5. SYNTHETIC MAREOGRAMS

In Figure 7 are shown the synthetic signals, obtained from (14) and (15), for a dip-slip mechanism with M_W=8.2; the focal depth are h_s=14 km (Fig. 6a) and h_s=34 km (Fig. 6b). We decide to account for source finiteness by properly weighting the point source spectrum using the scaling laws of Gusev (1983), as reported in Aki (1987). The structural model is model 3 of Section 4. For each of the two source-receiver distances considered the upper trace refers to the 1-D model and the lower trace to a laterally varying model. In the laterally varying model the liquid layer is getting thinner with increasing distance from the

source, with a gradient of 0.00175 and the uppermost solid layer is compensating this thinning. At 500 km from the source the effect of the lateral variation of the sea bottom is negligible and this is not surprising since, Δh, the difference in the thickness of the liquid layer between the 1-D and the 2-D models, is only of 1 km. After 2000 km from the source, Δh is equal to 3.5 km and the effects due to the variable bathymetry are clearly visible: 1) the 2-D wavetrain is arriving later than the 1-D wavetrain; 2) the amplitudes of the 2-D signals are generally larger. These effects can be explained by the dispersion of the tsunami mode: for a great range of periods (10000-200 s approximately) the phase and group velocities are directly proportional to the square root of the thickness of the liquid layer (see Figure 4), and when the tsunami mode is propagating in structures with a thinning liquid layer the differences between the velocities at the various periods become smaller, making the wavetrain more concentrated in time. The other factor which causes the slower decay of the amplitudes of the tsunami wavetrain is the conservation of the energy flux, since the wavetrain, as it propagates, is spread over thinner liquid layer.

In order to compare the theoretical parameters that can be extracted from synthetic signals with experimental ones, we show in Figure 8 the data set of Abe (1995) with the maximum amplitude curves (vertical component) calculated up to a epicentral distance of 2000 km, using both model 1 and model 3 of section 4, and a dip-slip source with the focal depth equal to 14 km and M_w equal to 8.1 and 7.7.

As a further example, we show some synthetic mareograms calculated for the tsunami mode propagating in a realistic model. The scheme of the laterally heterogeneous model considered is shown in Figure 9a, and represents a possible scenario for a tsunami excited by an earthquake generated at a subduction zone. In Figure 9b are shown the synthetic mareograms (vertical component) calculated at various distances along the section shown in Figure 9a for a lateral extension of zone C equal to 500 km. The elastic parameters of the crustal layer and of the half-space are those of model 3. The source has a dip-slip focal mechanism, focal depth of 16 km and M_W=8.0. In Figure 10 we show the maximum amplitude of the tsunami wavetrain (vertical component) versus epicentral distance, X, for different combinations of magnitude, mechanism and focal depth, that are

calculated using the structural model of Figure 9a. The comparison between the curves of Figure 10 and those shown in Figure 8 indicates that the lateral variations of the sea bottom can strongly modify the height of the Tsunami wavetrains, in terms of amplification or de-amplification according to the thinning or the thickening of the liquid layers.

6. CONCLUSIONS

The method developed allows us to calculate synthetic signals due to the tsunami mode, excited by a scaled double-couple source and propagating into an ocean, of variable thickness, fully coupled with the solid earth.

The increase of the tsunami wavetrain maximum amplitude in shallow water is caused not only by the conservation of the energy flux for a given frequency and then a distribution of the flux over a thinner water layer, but also by the decrease of the velocity dispersion at the frequencies corresponding to the maximum radiation.

Two main practical applications of our results are:

1) inversion of experimental tsunami recordings for some source parameters; the effectiveness of such an approach depends on the availability of tsunami measurements which are not heavily affected by unknown tide-gauges instrumental response or by harbour resonances: when tsunami records coming from pressure gauges in open ocean are available, some very long-period source characteristics can be revealed (Ritsema et al., 1995).

2) construction of a database for a quick system of tsunami warning; the calculated tsunami signals allow us to determine easily, for any source of interest, the maximum height of tsunami motion expected at different locations, taking into account the local variations of the sea bottom; these computations can of course be made before the event occurs, thus optimizing the efficiency of any warning system.

APPENDIX A. BOUNDARY CONDITIONS

The boundary condition at the free surface, equation (3), can be written as

$$\alpha_{-\ell}^2 \nabla \cdot \mathbf{u}_{-\ell} - g w_{-\ell} = 0 \qquad \text{(A1)}$$

or in matrix form

$$\mathbf{S}_{-\ell} \begin{pmatrix} A_{-\ell} \\ B_{-\ell} \end{pmatrix} = \begin{pmatrix} \rho_{-\ell}\alpha_{-\ell}^2 \left(-1 - \frac{g\eta_{1(-\ell)}}{\alpha_{-\ell}\omega^2} \right) & \rho_{-\ell}\alpha_{-\ell}^2 \left(1 + \frac{g\eta_{2(-\ell)}}{\alpha_{-\ell}\omega^2} \right) \end{pmatrix} \begin{pmatrix} A_{-\ell} \\ B_{-\ell} \end{pmatrix} = 0 \qquad \text{(A2)}$$

The boundary conditions at the interfaces between liquid layers correspond to the continuity of the vertical component of displacement, w and of the pressure, p, at the interface $z_{-j}+w_{-j}$ (since in an ideal fluid the condition of continuity of the tangential component of displacement is not required). We assume that the variation in depth of the interface has no effect on the boundary condition of the displacement and we accept continuity of w at $z= z_{-j}$ instead of $z= (z_{-j}+w_{-j})$, while for p the variation is taken into account at $z= z_{-j}$. The pressure increment due to the variation of the hydrostatic pressure is $g w_{-j}\left(\rho_{-j-1} - \rho_{-j}\right)$. Therefore we may assume that at the boundary $z=z_{-j}$ there is continuity of the quantity $\rho_{-j}\alpha_{-j}^2\left(\nabla \cdot \mathbf{u}_{-j}\right) - g\rho_{-j} w_{-j}$.

Using (7) and omitting the factor $\exp[i(\omega t - kr)]$, one obtains that

$$\begin{pmatrix} k w_{-j} \\ p_{-j} \end{pmatrix} = \mathbf{L}_{-j}\mathbf{K}_{-j} \begin{pmatrix} A_{-j} \\ B_{-j} \end{pmatrix} \qquad \text{(A3)}$$

where

$$\mathbf{L}_{-j} = \begin{pmatrix} -\frac{\alpha_{-j}\psi_{-j}}{c} - \frac{g}{2\omega c} & -\frac{\alpha_{-j}\psi_{-j}}{c} + \frac{g}{2\omega c} \\ -\rho_{-j}\alpha_{-j}^2 \left(1 + \frac{g\eta_{1(-j)}}{\alpha_{-j}\omega^2} \right) & \rho_{-j}\alpha_{-j}^2 \left(1 + \frac{g\eta_{2(-j)}}{\alpha_{-j}\omega^2} \right) \end{pmatrix} \qquad \text{(A4)}$$

$$\mathbf{K}_{-j} = \begin{pmatrix} \exp\left(-\frac{H_{-j}\eta_{2(-j)}}{\alpha_{-j}}\right) & 0 \\ 0 & \exp\left(-\frac{H_{-j}\eta_{1(-j)}}{\alpha_{-j}}\right) \end{pmatrix} \tag{A5}$$

and H_{-j} is the thickness of the j-th liquid layer. The layer matrix, which relates the vertical component of displacement and the normal stress in the j-th liquid layer with the same quantities in the j+1-th liquid layer, is:

$$\mathbf{D}_{-j} = \mathbf{L}_{-j}\mathbf{K}_{-j}^{-1}\mathbf{L}_{-j}^{-1} \tag{A6}$$

The relationship between the coefficients in (7) for the uppermost liquid layer and those for the first liquid layer, can be found using (A3) and (A6):

$$\begin{pmatrix} A_{-\ell} \\ \\ B_{-\ell} \end{pmatrix} = \mathbf{L}_{-\ell}^{-1}\mathbf{D}_{-\ell}\mathbf{D}_{-\ell+1}\cdots\mathbf{D}_{-2}\mathbf{L}_{-1}\begin{pmatrix} A_{-1} \\ \\ B_{-1} \end{pmatrix} \tag{A7}$$

and the boundary condition (A1) can be written:

$$\mathbf{S}_{-\ell}\mathbf{L}_{-\ell}^{-1}\mathbf{D}_{-\ell}\mathbf{D}_{-\ell+1}\cdots\mathbf{D}_{-2}\mathbf{L}_{-1}\begin{pmatrix} A_{-1} \\ \\ B_{-1} \end{pmatrix} = \mathbf{M}\begin{pmatrix} A_{-1} \\ \\ B_{-1} \end{pmatrix} = 0 \tag{A8}$$

The expression for the pressure in the last liquid layer (1-st in Fig. 1) is:

$$p_{-1} = \rho_{-1}\alpha_{-1}^2\nabla\cdot\mathbf{u}_{-1} = \mathbf{R}\begin{pmatrix} A_{-1} \\ B_{-1} \end{pmatrix} \tag{A9}$$

and the expression for the vertical component of displacement can be written in the same form:

$$kw_{-1} = \frac{\alpha_{-1}}{c\omega}\left(\eta_{1(-1)} \quad -\eta_{2(-1)}\right)\mathbf{K}_{-1}\begin{pmatrix} A_{-1} \\ B_{-1} \end{pmatrix} = \mathbf{P}\begin{pmatrix} A_{-1} \\ B_{-1} \end{pmatrix} \tag{A10}$$

The boundary conditions (5a-5b) at the liquid solid interface can be written, using (9), (A9) and (A10), in the following matrix notation:

$$\begin{pmatrix} \frac{r_{\alpha 1}\alpha_1}{c} & -\frac{r_{\alpha 1}\alpha_1}{c} & -\frac{\beta_1^2}{c^2} & \frac{\beta_1^2}{c^2} \\ \rho_1\alpha_1^2\left(1-\frac{2\beta_1^2}{c^2}\right) & \rho_1\alpha_1^2\left(1-\frac{2\beta_1^2}{c^2}\right) & \frac{2\mu_1\beta_1 r_{\beta 1}}{c} & \frac{2\mu_1\beta_1 r_{\beta 1}}{c} \end{pmatrix}\begin{pmatrix} C_1 \\ D_1 \\ E_1 \\ F_1 \end{pmatrix} =$$

$$= \begin{pmatrix} p_1 & p_2 \\ r_1 & r_2 \end{pmatrix}\begin{pmatrix} A_{-1} \\ B_{-1} \end{pmatrix} \tag{A11}$$

From (A8), containing the matrix $\mathbf{M}=(m_1, m_2)$, one obtains

$$A_{-1} = -m_2 K \qquad B_{-1} = m_1 K \tag{A12}$$

where K is an unknown multiplier, and the right-hand side of (A11) can be written in the following form:

$$\mathbf{F}K = \begin{pmatrix} f_1 \\ f_2 \end{pmatrix}K = \begin{pmatrix} -p_1 m_2 + p_2 m_1 \\ -r_1 m_2 + r_2 m_1 \end{pmatrix}K \tag{A13}$$

The two equations (A11) can be reduced to one for the coefficients of the first solid layer, and considering the condition (5c) one has:

$$\mathbf{C}\begin{pmatrix} C_1 \\ D_1 \\ E_1 \\ F_1 \end{pmatrix} = 0 \tag{A14}$$

where **C** is a (2×4) matrix and the problem is now formally equivalent to that for a system of solid layers, where (A14) replaces the condition of free surface, and the dispersion function can be constructed using either Haskell (1953) or Knopoff (1964) method.

APPENDIX B. HASKELL AND KNOPOFF METHODS

After some manipulations equation (A14) can be transformed to

$$\tilde{C}\begin{pmatrix} C_1 \\ D_1 \\ E_1 \\ F_1 \end{pmatrix} = 2f_1\rho_1^2 c^4 \gamma_1 \begin{pmatrix} (1-\gamma_1) & q/(\rho_1 c^2) & -\gamma_1 & -q\rho_1 c^2 \\ 0 & \gamma_1 & 0 & -(1-\gamma_1) \end{pmatrix} \begin{pmatrix} C_1 \\ D_1 \\ E_1 \\ F_1 \end{pmatrix} = 0 \qquad \text{(B1)}$$

where ρ_1 is the density of the uppermost solid layer, $\gamma_1 = 2\beta_1^2 / c^2 - 1$ and $q = f_2/f_1$. Following Schwab (1970), from (B1) the matrix $\mathbf{T}_0$ can be extracted:

$$\mathbf{T}_0 = \left(\gamma_1(1-\gamma_1) \quad 0 \quad (1-\gamma_1)^2 \quad \gamma_1^2 \quad q/\rho_1 c^2 \quad \gamma_1(\gamma_1 - 1)\right) \qquad \text{(B2)}$$

and Knopoff's algorithm (Schwab and Knopoff, 1972) can be immediately applied.

In order to derive the dispersion equation by Haskell (1953) method we start from (A13). At the interface between the m-th and (m+1)-th solid layer, applying the boundary conditions (6) to expressions (7) we obtain:

$$\mathbf{L}_m\mathbf{K}_m\begin{pmatrix} C_m \\ D_m \\ E_m \\ F_m \end{pmatrix} = \mathbf{L}_{m+1}\begin{pmatrix} C_{m+1} \\ D_{m+1} \\ E_{m+1} \\ F_{m+1} \end{pmatrix} \tag{B3}$$

where the matrices $\mathbf{L}_m$ and $\mathbf{K}_m$ are:

$$\mathbf{L}_m = \begin{pmatrix} \frac{\alpha_m^2}{c^2} & \frac{\alpha_m^2}{c^2} & -\frac{\beta_m r_{\beta m}}{c} & -\frac{\beta_m r_{\beta m}}{c} \\ \frac{\alpha_m r_{\alpha m}}{c} & -\frac{\alpha_m r_{\alpha m}}{c} & -\frac{\beta_m^2}{c^2} & \frac{\beta_m^2}{c^2} \\ -\frac{2\mu_m\alpha_m r_{\alpha m}}{c} & \frac{2\mu_m\alpha_m r_{\alpha m}}{c} & \mu_m(\gamma_m - 1) & -\mu_m(\gamma_m - 1) \\ -\rho_m\alpha_m^2(\gamma_m - 1) & -\rho_m\alpha_m^2(\gamma_m - 1) & \frac{2\mu_m\beta_m r_{\beta m}}{c} & \frac{2\mu_m\beta_m r_{\beta m}}{c} \end{pmatrix} \tag{B4}$$

$$\mathbf{K}_m = \begin{pmatrix} \exp\left(-\frac{\omega r_{\alpha m} H_m}{\alpha_m}\right) & 0 & 0 & 0 \\ 0 & \exp\left(\frac{\omega r_{\alpha m} H_m}{\alpha_m}\right) & 0 & 0 \\ 0 & 0 & \exp\left(-\frac{\omega r_{\beta m} H_m}{\beta_m}\right) & 0 \\ 0 & 0 & 0 & \exp\left(\frac{\omega r_{\beta m} H_m}{\beta_m}\right) \end{pmatrix}$$

Using recursively (B3), the relationship between the coefficients of (9) in the first solid layer and the coefficients in the half-space (n-th layer) can be written as:

$$\begin{pmatrix} C_1 \\ D_1 \\ E_1 \\ F_1 \end{pmatrix} = \mathbf{L}_1^{-1}\mathbf{D}_2 \ldots \mathbf{D}_{n-1}\mathbf{L}_n\begin{pmatrix} C_n \\ E_n \end{pmatrix} \tag{B5}$$

where the matrix $\mathbf{L}_n$ (4×2) contains the 1st and the 3rd columns of the matrix $\mathbf{L}$, and the layer matrix is $\mathbf{D}_m = \mathbf{L}_m\mathbf{K}_m^{-1}\mathbf{L}_m^{-1}$ (m=2,...,n-1). Using (A13), one obtains (13) where all of the matrices appearing are real.

APPENDIX C: FORMULAS FOR THE TRAVEL TIME AND THE GEOMETRICAL SPREADING

If the phase velocity, c(x), varies linearly along the x-axis, i.e. $c=c_0(1+\varepsilon x)$, and if at $x_0=0$ the angle between the wave direction of propagation and the x axis is θ_0 (see Fig. 2b), then at x=X:

$$Y = \frac{(\cos\theta_0 - \cos\theta)}{\varepsilon \sin\theta_0} \tag{C1}$$

$$\tau = \frac{\left[\cosh^{-1}(1/\sin\theta) - \cosh^{-1}(1/\sin\theta_0)\right]}{\varepsilon\, c_0} \tag{C2}$$

$$J = \frac{Y}{\sin\theta_0} \tag{C3}$$

while if the wave is propagating along x-axis, so that $\theta_0=0$ and Y=0, at x=X:

$$\tau = \frac{\log(1+\varepsilon X)}{\varepsilon\, c_0} \tag{C4}$$

$$J = \left(1+\frac{\varepsilon X}{2}\right)X \tag{C5}$$

If c(x) is a piece-wise linear function the travel time is calculated by the summation of the expressions (C.2) or (C.4) and the expressions for the geometrical spreading become:

$$J=\begin{cases}\dfrac{\cos\theta_0\cos\theta_n}{\sin\theta_0}\displaystyle\sum_{i=1}^{n}\frac{y_i}{\cos\theta_i\cos\theta_{i-1}} & \theta_0\neq 0\\ \displaystyle\sum_{i=1}^{n}\frac{c_{i-1}}{c_0}\left(1+\frac{\varepsilon_i x_i}{2}\right)x_i & \theta_0=0\end{cases} \qquad \text{(C6)}$$

where the y_i (i=1,...,n) are calculated using formula (C1) at $x=x_i$.

To justify the assumption that θ_0 can be considered equal to zero, we calculate the travel times and the geometrical spreading using formulas (C2-C4) and (C3-C5) under the assumption that the velocity varies in the direction OX (see Fig. 2b). Assuming a velocity variation similar to that used in this study (from 0.2 km/s at x=0 to 0.014 km/s at X=2000 km) the difference in the geometrical spreading evaluated by formulas (C6) is about 5% for θ_0 =46°, and 10% for θ_0 =64°. Such difference is obtained at low frequencies, for which the difference in velocities due to the decrease of the thickness of the water layer is maximum. For higher frequencies the difference in velocities decreases, and the effect is even smaller.

Estimation of the difference in the arrival times for the same models shows that the signal arrives 100s earlier if θ_0=25°, and 1000s earlier if θ_0=72°. This does not lead to a significant difference with respect to the signals calculated for normal incidence, even if the take-off angle with respect to the x-axis is sufficiently large (~60-70°).

ACKNOWLEDGEMENTS

We acknowledge the useful comments of Dr. Stephen Ward that allowed us to clarify the basic assumptions of our modelling. We acknowledge financial support from GNDT (contract 94.01703.PF54), MURST (40% and 60% funds), EEC Contract EV5V-CT94-0491.

REFERENCES

A.A.V.V., 1989. *Seismic surface waves in a laterally heterogeneous Earth*, (V. I. Keilis-Borok editor), Kluwer Academic Publishers, Dordrecht.

Abe, K., 1995. Estimate of tsunami run-up heights from earthquake magnitudes, in *Tsunami: progress in prediction, disaster prevention and warning*, (Y. Tsuchiya and N. Shuto ed.), Kluwer Academic Publishers, Dordrecht, pp.21-35.

Aki, K, 1987. Strong motion seismology, in M. Erdik and M. Toksöz (eds) *Strong ground motion seismology*, NATO ASI Series, Series C: Mathematical and Physical Sciences, D. Reidel Publishing Company, Dordrecht, Vol. 204, pp. 3-39.

Aki, K. & Richards, P. G., 1980. Quantitative Seismology, Freeman & Co., San Francisco.

Comer, R. P., 1984. The tsunami mode of a flat earth and its excitation by earthquake sources, *Geophys. J. R. Astr. Soc.*, 77, 1-27.

Florsch, N., Fäh, D., Suhadolc, P. and G. F. Panza, 1991. Complete synthetic seismograms for high-frequency multimode SH-waves, *PAGEOPH*, **136**, 529-560.

Gusev, A. A., 1983. Descriptive statistical model of earthquake source radiation and its application to an estimation of short period strong motion, *Geophys. J. R. Astron. Soc.* **74**, 787-800.

Haskell, N. A., 1953. The dispersion of surface waves in multilayered media, *Bull. Seism. Soc. Am.*, **43**, 17-34.

Knopoff, L., 1964. A matrix method for elastic wave problems, *Bull. Seism. Soc. Am.*, **54**, 431-438.

Panza, G. F., Schwab F. A., and L. Knopoff, 1973. Multimode surface waves for selected focal mechanisms. I. Dip-slip sources on a vertical fault plane, *Geophys. J. R. Astr. Soc.*, **34**, 265-278.

Panza, G. F., 1985. Synthetic seismograms: the Rayleigh waves modal summation, *J. Geophys.*, **58**, 125-145.

Panza, G. F., and P. Suhadolc, 1987. Complete strong motion synthetics. In *Seismic strong motion synthetics* (B. A. Bolt editor), Academic Press, Orlando, 153-204.

Pod'yapolsky, G.S., 1968. Generation of longperiodic gravitational wave in the ocean by seismic source in the crust, *Izvestia AN SSSR, Fizika Zemli*, **1**, 7-24 (in Russian).

Pod'yapolsky G.S., 1970. Generation of the tsunami wave by the earthquake, in *Tsunamis in the Pacific Ocean*, pp.19-32, ed. Adams W..M., East-West Center Press, Honolulu.

Ritsema, J., Ward, S. and F. I. Gonzalez, 1995. Inversion of deep-ocean tsunami records for 1987 to 1988 gulf of Alaska earthquake parameters, *Bull. Seism. Soc. Am.*, **85**, N. 3, 747-754.

Schwab, F. A., 1970. Surface-wave dispersion computations: Knopoff's method, *Bull. Seism. Soc. Am.*, **60**, 1491-1520.

Schwab, F. A., and L. Knopoff, 1972. Fast surface wave and free mode computations, in *Methods in computational Physics* (B. A. Bolt editor), Academic Press, New York, 86-180.

Ward, S. N., 1980. Relationships of tsunami generation and an earthquake source, *J. Phys. Earth*, **28**, 441-474.

Ward, S. N., 1981. On tsunami nucleation: I. A point source, *J Geophys. Res.*, **86**, 7895-7900.

Ward, S. N., 1982a. On tsunami nucleation: II. An instantaneous modulated line source, *Phys. Earth Planet. Int.*, **27**, 273-285.

Ward, S. N., 1982b. Earthquake mechanisms and tsunami generation: the Kurile Islands event of October 13, 1963, *Bull. Seism. Soc. Am.*, **72**, 759-778.

Ward, S. N., 1989. Tsunamis, in *The encyclopaedia of solid earth geophysics* (D. E. James editor), Van Nostrand Reinhold company, New York, 1279-1292.

FIGURE CAPTIONS

Figure 1. Reference system for the laterally homogeneous (1-D) model.

Figure 2. Reference system for the laterally heterogeneous model. a) Lateral view; b) top view. The star and the triangle represent respectively the source and the receiver site position.

Figure 3. Amplitude spectra calculated for a double–couple source (10^{13} N m seismic moment) at 500 km from the receiver. a) Radial (x) and vertical (z) components of motion for pure strike-slip (ss) and pure dip-slip (ds) mechanisms; b) radial and vertical components for a liquid layer 4, 6 and 8 km thick.

Figure 4. Phase (p) and group (g) velocities dispersion curve of the tsunami mode for three values of the thickness of the liquid layer: 4 (solid lines), 6 (dashed lines) and 8 (dotted lines) km.

Figure 5. Amplitude spectra calculated for a double–couple source (10^{13} N m seismic moment) using model 1 (a), model 2 (b) and model 3 (c) (see text for the elastic parameters information). In each case, two focal depths, 9 and 14 km (second part of the acronym), and two source-receiver distance, 500 and 2000 km (third part of the acronym), are shown.

Figure 6. a) Eigenfunctions of the radial (solid line) and vertical (dotted line, normalized to 1 at the free-surface) component of motion at frequency equal to 0.007 Hz, in the fluid. The curves for the models 1, 2 and 3, are totally overlapped; b) eigenfunctions in the solid layers.

Figure 7. Synthetic signals for the tsunami mode (vertical component) excited by a dip-slip mechanism with M_0=2.2 10^{21} Nm. a) h_S = 14 km; b) h_S = 34 km. For each source-receiver distance, X, the upper trace refers to the 1-D model and the lower trace to the 2-D model.

Figure 8. Curves of the maximum height of the calculated tsunami signal (vertical component) versus the epicentral distance. Each acronym shows the 1-D model (1 or 3) and the magnitude (M_w) adopted in the calculations. The symbols the experimental points, for two different magnitudes (squares for M_s=8.1, circles for M_s=7.7), shown by Abe (1995).

Figure 9. a) Sketch of the laterally heterogeneous model for a realistic scenario. The numbers refer to the thickness (km) of the water, of the crustal layer and, to the lateral extension of each zone. b) Synthetic mareograms (vertical component) calculated at various distances along the section shown in a). The extension of zone C is 500 km.

Figure 10. Curves of the maximum height of the calculated tsunami signal (vertical component) versus the epicentral distance. Each acronym shows the focal mechanism (ds indicates for dip-slip, ss strike-slip), the focal depth (km) and the magnitude (M_w) adopted in the calculations. The model adopted in the calculations is shown in Figure 9a.

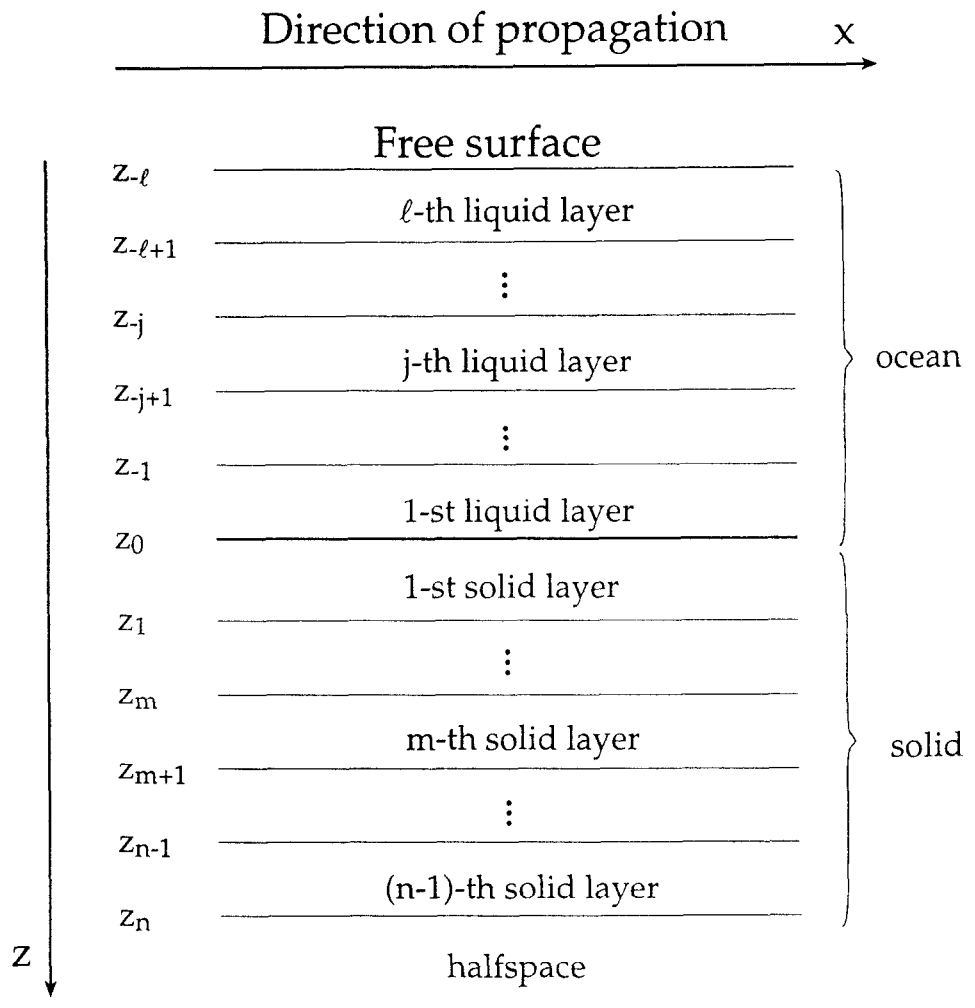

Figure 1. Reference system for the laterally homogeneous (1-D) model.

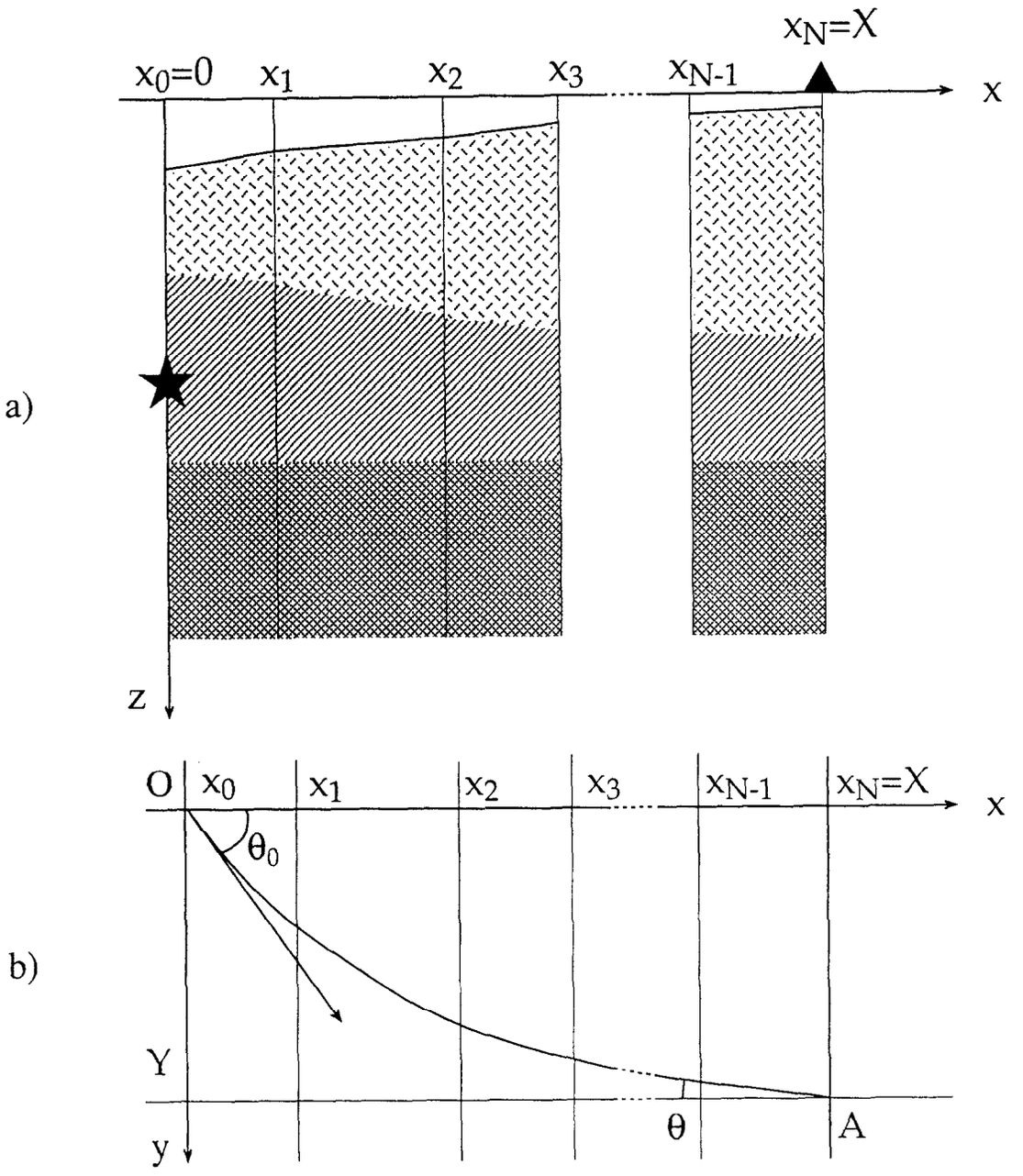

Figure 2. Reference system for the laterally heterogeneous model.
a) lateral view; b) top view. The star represents the source and the triangle the receiver site.

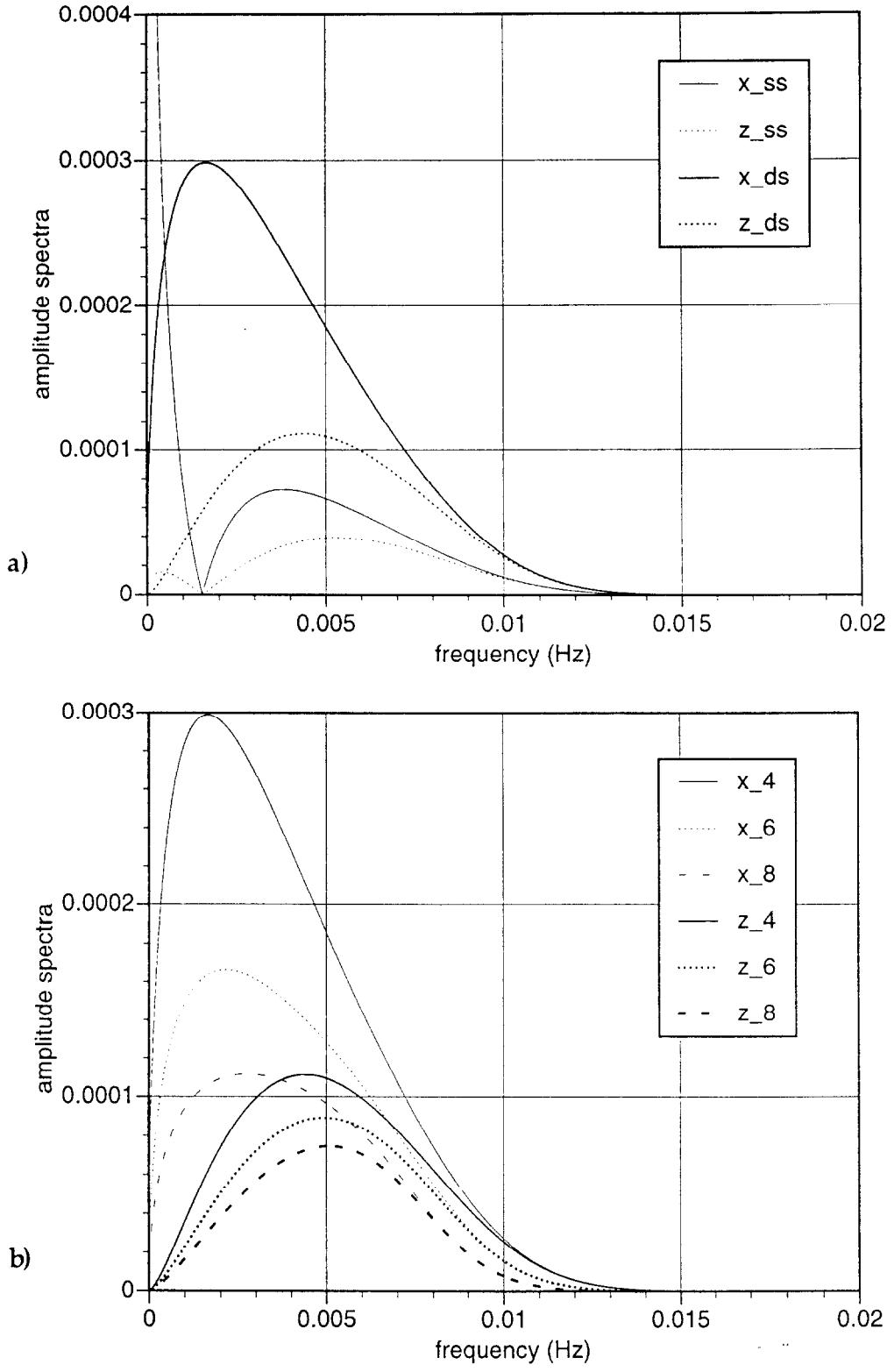

Figure 3. Amplitude spectra calculated for a double-couple source (10^{13} Nm seismic moment) at 500 km from the receiver. a) radial (x) and vertical (z) components of motion for pure strike-slip (ss) and pure dip-slip (ds) mechanisms; b) radial and vertical components for a liquid layer 4, 6 and 8 km thick.

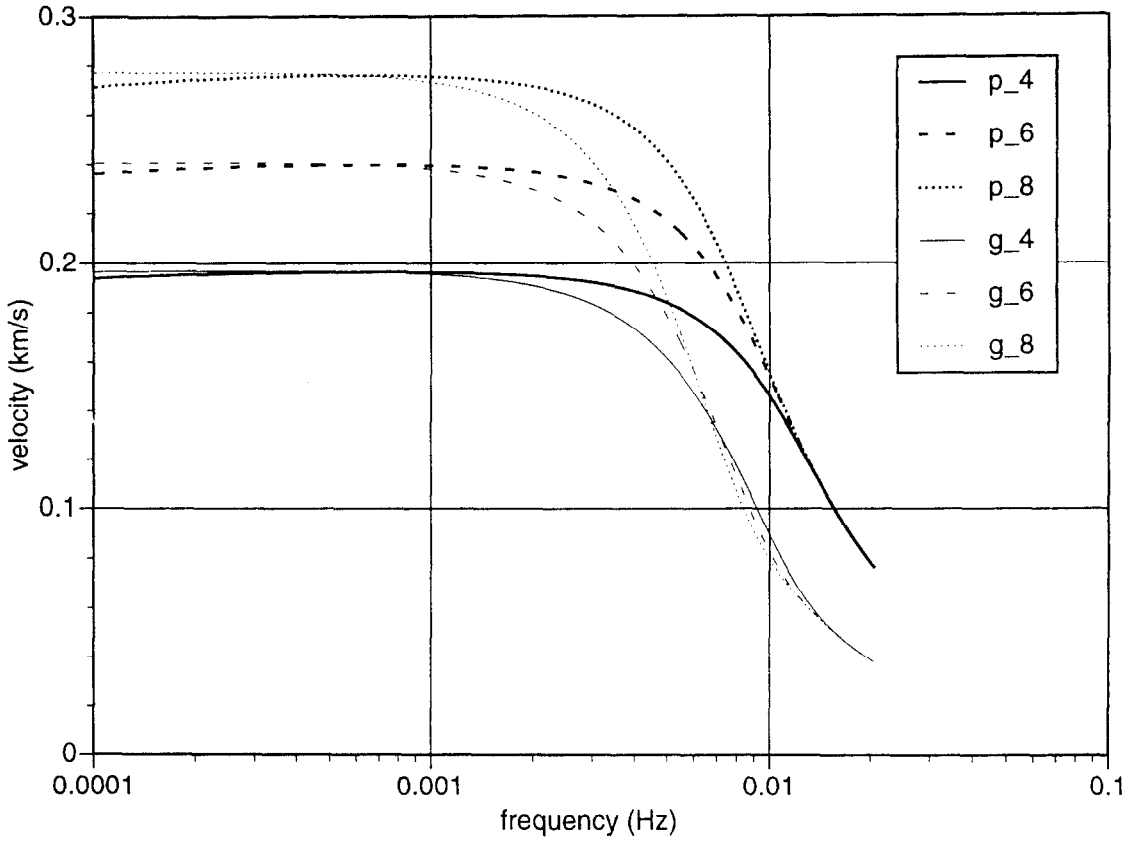

Figure 4. Phase (p) and group (g) velocities dispersion curve of the tsunami mode for three values of the thickness of the liquid layer: 4 (solid lines), 6 (dashed lines) and 8 (dotted lines) km.

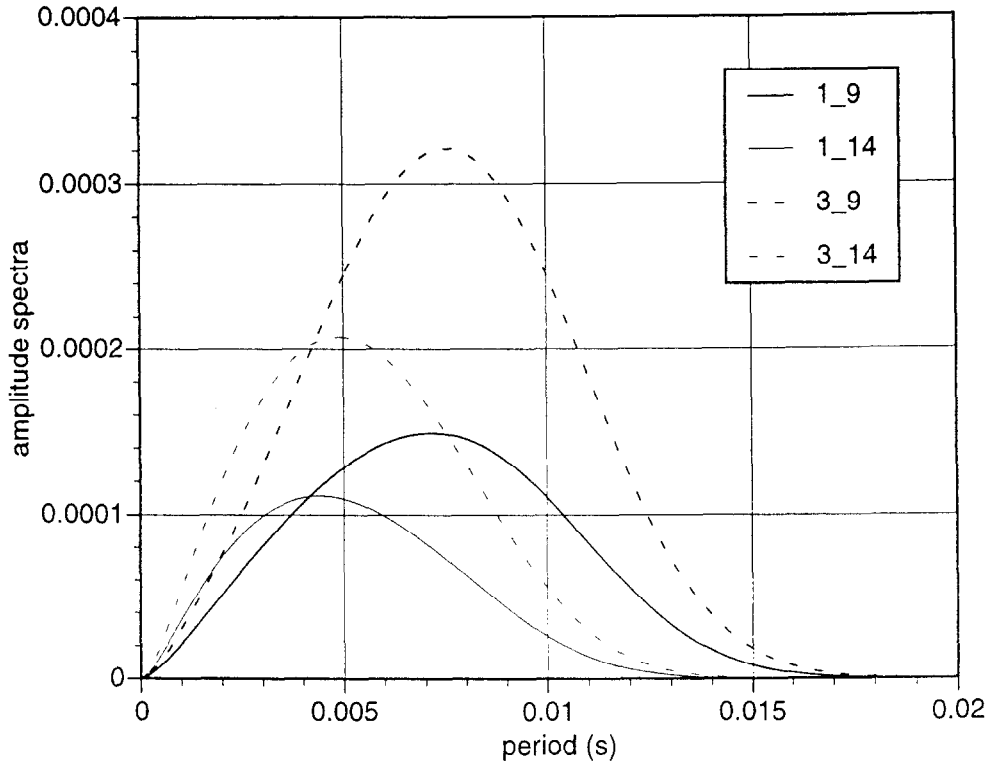

Figure 5. Amplitude spectra (vertical component of motion) calculated for a dip-slip double-couple source (10^{13} Nm seismic moment) using model 1 and model 3 (see text for the elastic parameters specification). The source-receiver distance is 500 km and two focal depths, 9 and 14 km (second part of the acronym) are shown.

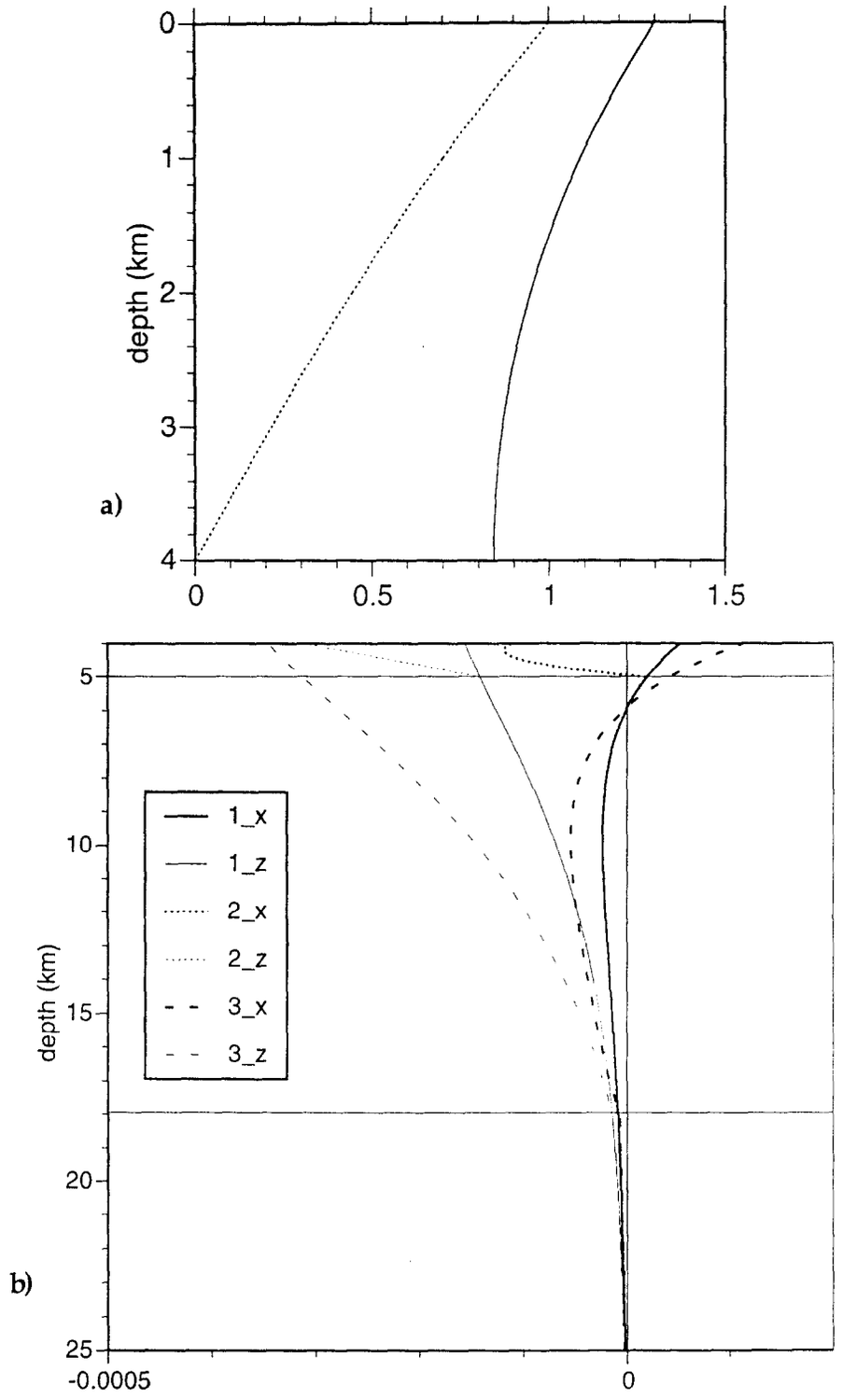

Figure 6. a) Eigenfunctions of the radial (solid line) and vertical (dotted line, normalized to 1 at the free-surface) component of motion at frequency equal to 0.007 Hz, in the fluid. The curves for the models 1, 2 and 3, are totally overlapped; b) eigenfunctions in the solid layers.

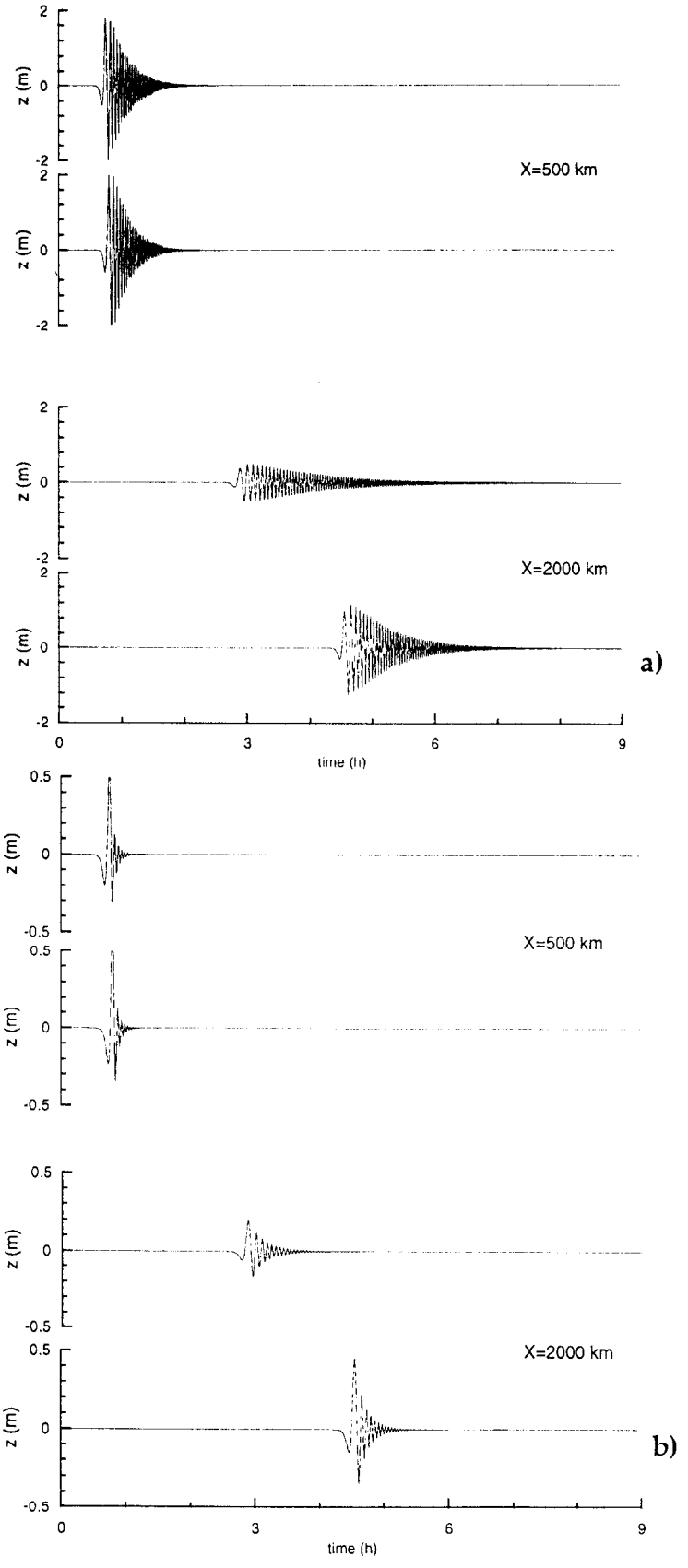

Figure 7. Synthetic signals for the tsunami mode (vertical component) excited by a dip-slip mechanism with M_0=2.2 10^{21} Nm. a) h_S = 14 km; b) h_S = 34 km. For each source-receiver distance, X, the upper trace refers to the 1-D model and the lower trace to the 2-D model.

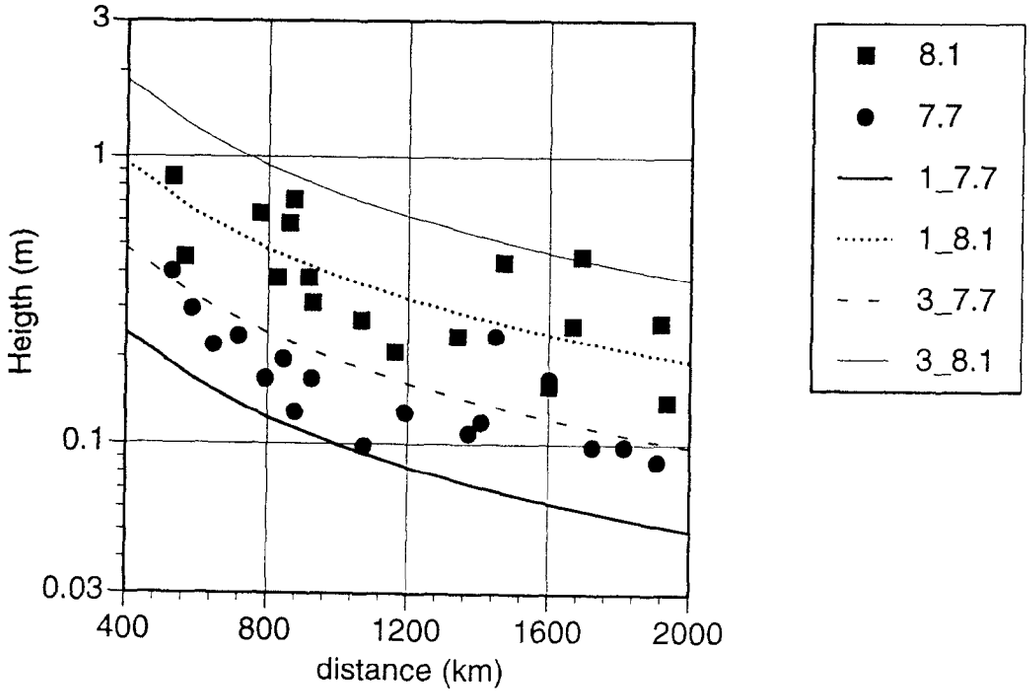

Figure 8. Curves of the maximum height of the calculated tsunami signal (vertical component) versus the epicentral distance. Each acronym shows the 1-D model (1 or 3) and the magnitude (M_w) adopted in the calculations. The symbols the experimental points, for two different magnitudes (squares for M_s=8.1, circles for M_s=7.7), shown by Abe (1995).

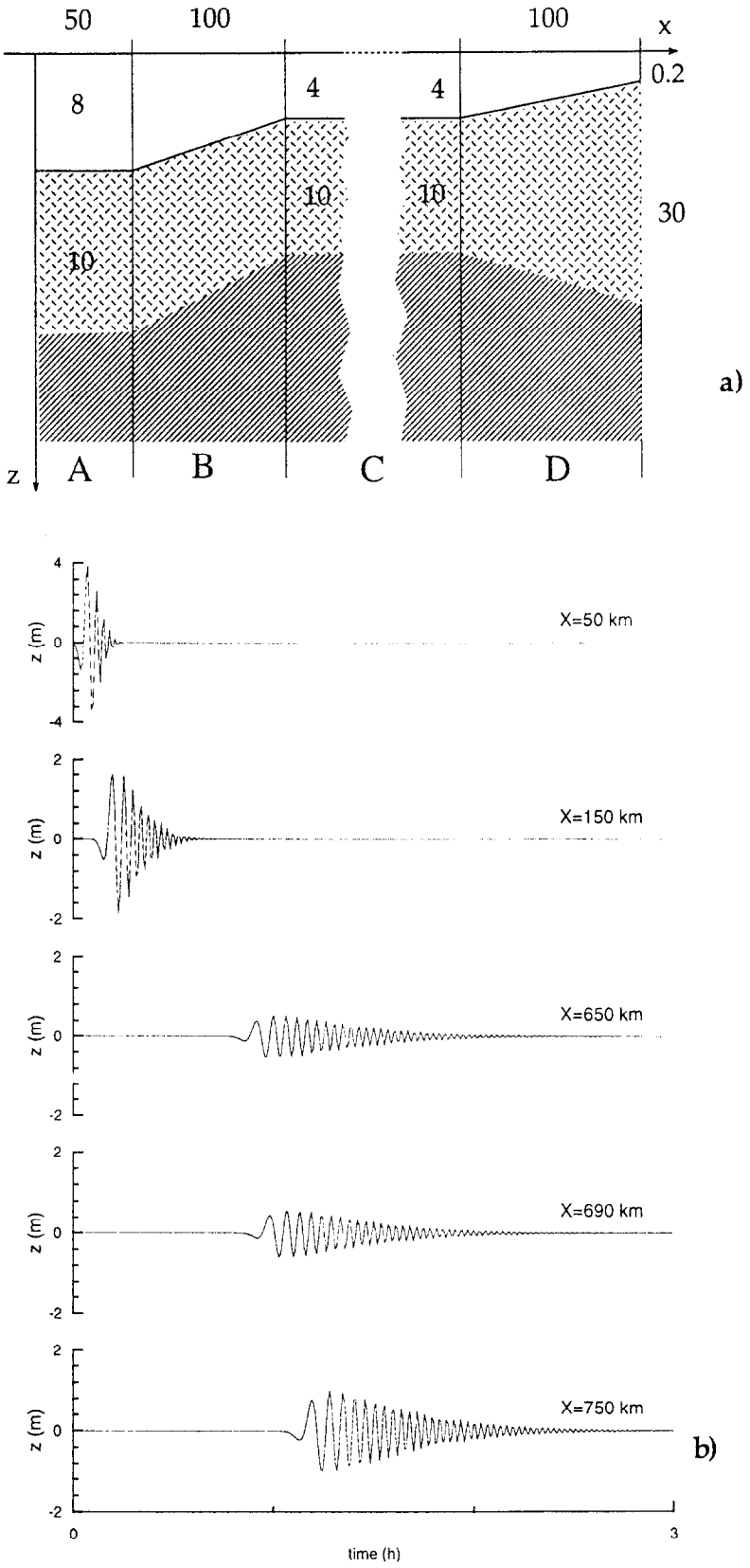

Figure 9. a) Sketch of the laterally heterogeneous model for a realistic scenario. The numbers refer to the thickness (km) of the water, of the crustal layer and, to the lateral extension of each zone. b) Synthetic mareograms (vertical component) calculated at various distances along the section shown in a). The extension of zone C is 500 km.

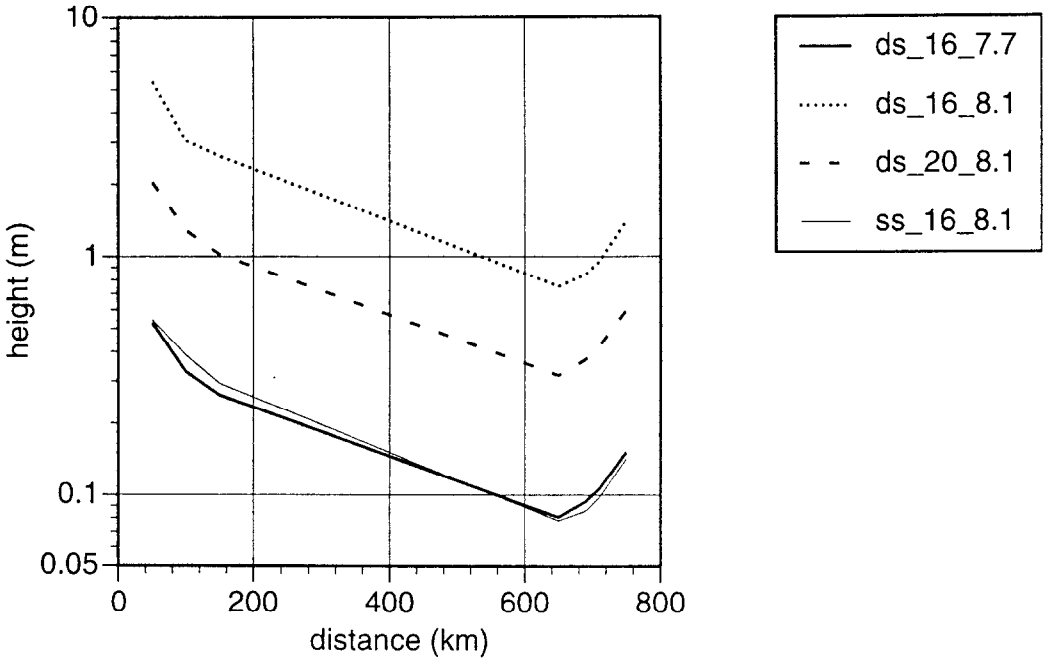

Figure 10. Curves of the maximum height of the calculated tsunami signal (vertical component) versus the epicentral distance. Each acronym shows the focal mechanism (ds indicates for dip-slip, ss strike-slip), the focal depth (km) and the magnitude (M_w) adopted in the calculations. The model adopted in the calculations is shown in Figure 9a.